Ab Initio Investigation of the Auger Spectra of Methane, Ethane, Ethylene, and Acetylene

Florian Matz,* Jonas Nijssen, and Thomas-Christian Jagau

Department of Chemistry, KU Leuven, B-3001 Leuven, Belgium

E-mail: florian.matz@kuleuven.be

Abstract

We present an *ab initio* computational study of the Auger spectra of methane, ethane, ethylene, and acetylene. Auger spectroscopy is an established technique to probe the electronic structure of molecules and exploits the Auger-Meitner effect that core-ionized states undergo. We compute partial decay widths using coupled-cluster theory with single and double substitutions (CCSD) and equation-of-motion-CCSD theory combined with complex-scaled basis functions and Feshbach-Fano projection. We generate Auger spectra from these partial widths and draw conclusions about the strength of particular decay channels and trends between the four molecules. A connection to experimental results about fragmentation pathways of the electronic states produced by Auger decay is also made.

Introduction

Carbon atoms in different hybridization states and chemical environments are the basic building blocks of organic chemistry. There is ample evidence that an analysis of the core-vacant states produced by X rays, specifically through the measurement of the energies of Auger electrons, can yield important information about chemical properties, electronic structure, and molecular geometry of organic compounds.[1–8] In Auger decay, a core vacancy is filled by one valence electron, while a second valence electron — the Auger electron — is simultaneously emitted into the continuum.[9,10] This is the dominant relaxation mechanism of core vacancies in systems with light nuclei, i.e., nuclei lighter than about germanium for K-shell holes and lighter than about neptunium for L-shell holes.[11,12]

Core vacancies include core-ionized states, which are the focus of this manuscript, and core-excited states where one usually speaks of resonant Auger decay.[13,14] Furthermore, processes that change the internal energy of a molecule as strongly as core ionization and Auger decay tend to produce satellite or shake-up states, in which valence electrons are excited in addition to the relaxation of the core hole. These satellite states enable additional decay

channels. A particular example is double Auger decay,[15] where two electrons are simultaneously emitted from a system with a core vacancy. In the present manuscript, however, we do not consider satellite states and focus on those target states that are characterized by exactly two holes in the valence region. Decay into these states usually dominates molecular Auger spectra.

While Auger spectroscopy of small organic molecules such as methane, ethane, ethylene, and acetylene has been the subject of experimental and theoretical studies for many years,[16–31] recent advances in X-ray technology and computational methods have driven renewed interest in the field.[32–45] Many previous works focused on differentiating between final states of Auger decay in terms of fragmentation processes, but the computation of total and partial Auger decay widths has remained a challenge due to the necessity to deal with the ionization continuum and a multitude of final states.

Core-ionized states are electronic resonances and their decay is not captured by quantum-chemical methods designed for bound states.[46,47] In most computations on core-vacant states, Auger decay is neglected by invoking the core-valence separation[48] (CVS), where configurations in which the core hole is filled are projected out from the wave function. Due to the energetic separation of core and valence orbitals, the contribution of these configurations to the wave function is small and CVS methods enable reliable calculation of energies of core-vacant states.[49–54]

Computations of Auger decay widths usually rely on the Wentzel approach,[55,56] which means that the decay of a core vacancy is independent of the mechanism by which it is created. One possible technique is the Feshbach-Fano method, where the Hilbert space is partitioned into bound and continuum configurations.[57–59] The bound part of the core-vacant state is not subject to decay; one can use, for example, CVS to define it. Greater difficulty lies in defining appropriate wave functions for the continuum part. Using Stieltjes imaging, the continuum functions can be constructed in an implicit fashion;[60,61] alternatively, it is possible to construct the wave function of the Auger electron explicitly.[42,43,62–66] A possible

approach to facilitate Feshbach-Fano calculations is the one-center approximation.[42–44,62,67] Here, electron-repulsion integrals involving continuum functions, which are necessary for the computation of the width, are approximated by a linear combination of the respective integrals for Auger decay in isolated atoms.

The Feshbach-Fano method has been combined with several electronic-structure methods including algebraic diagrammatic construction,[68,69] multireference configuration-interaction,[44,63,64] and equation-of-motion coupled-cluster theory with single and double substitutions (EOM-CCSD).[65,66] The latter approach, which we dub Fano-EOM-CCSD in the following, is used in this work.

As an alternative to Fano-EOM-CCSD, we use complex-scaled basis functions[70–73] (CBFs) combined with CCSD and EOM-CCSD theory. The CBF approach is related to complex scaling[74,75] and has been shown to yield accurate total and partial Auger decay widths.[76–78] CBF methods are capable of describing the bound and unbound parts of a resonance state at once; there is no need to partition the Hilbert space or to impose an explicit form for the wave function of the Auger electron.

In the following section, we discuss the theory of total and partial Auger decay widths and the methods used for their computation. Subsequently, we present our numerical results for the Auger decay widths of methane, ethane, ethylene, and acetylene and construct their Auger spectra. The last section offers our concluding remarks on the *ab initio* computation of Auger spectra.

Theoretical construction of Auger spectra

The simulation of Auger electron spectra requires two quantities for each decay channel i: the kinetic energy of the Auger electrons (E_i) and the decay rate, which is proportional to the partial decay width Γ_i. Our two approaches for computing these quantities are shown in Figure 1 and explained in the following.

Due to energy conservation, the energy of an Auger electron is given as the difference

$$E_i = E(\mathrm{A}^{+*}) - E(\mathrm{A}_i^{2+}) \tag{1}$$

between the energy of the core-ionized initial state $E(\mathrm{A}^{+*})$ and that of the doubly-ionized target state $E(\mathrm{A}_i^{2+})$. To obtain these energies, EOM-CC methods[79–83] are particularly useful because they enable the computation of energies of states with a different number of electrons using the same Hamiltonian and orbital set. In our calculations, we use the CCSD approximation and take the neutral ground state of every molecule as the reference.

We compute the energies of the initial states with EOM-ionization potential-CCSD (EOMIP-CCSD),[84] the corresponding wave functions are constructed by applying single hole ($1h$) and two-hole-one-particle ($2h1p$) excitation operators to the CCSD reference wave function. The energies of the target states, which have two electrons fewer than the reference state, are computed with the EOM-double ionization potential-CCSD (EOMDIP-CCSD) method,[85,86] which includes two hole ($2h$) and three-hole-one-particle ($3h1p$) excitation operators.

Determination of Auger decay widths with complex-variable methods

We previously demonstrated that total and partial Auger decay widths can be extracted from CBF-EOMIP-CCSD wave functions of core-ionized states.[76–78] The decay is represented in these wave functions by $2h1p$-excitations that fill the core hole. The resulting configurations give rise to the metastable character and are responsible for convergence problems when methods are used that do not treat the decay properly.[49,52] With CBF methods, however, the decay can be captured. Here, selected Gaussian basis functions have an exponent scaled by a complex number $\mathrm{e}^{-2\mathrm{i}\theta}$.[70] The Hamiltonian constructed in such a basis set has complex

energy eigenvalues

$$E_{\mathrm{res}} = E - \mathrm{i}\,\frac{\Gamma}{2}\,. \tag{2}$$

From the imaginary part, the total decay width Γ is obtained, while the real part E represents the physical energy in the usual sense.

To obtain the partial width for a channel, we solve the EOMIP-CCSD equations for the core-ionized state under the constraint that the amplitudes for this particular channel are zero, which we previously referred to as Auger Channel Projector (ACP).[77] The difference in the total width with and without the channel being present is then interpreted as partial width.

Alternatively, it is possible to determine Auger decay widths from a CBF-CCSD calculation on the core-ionized state.[76] The total decay width is obtained from the imaginary part of the CCSD energy corrected by the value obtained for the closed-shell ground state. This procedure is referred to as ΔCCSD. To obtain partial widths in this approach, the imaginary CCSD energy is decomposed into contributions from the decay channels. These are again represented by doubly excited determinants in which the core hole is filled. The partial widths obtained from this approach are strictly additive unlike those obtained from the ACP approach where other channels can react to the removal of a particular decay channel, which can result in unphysical contamination.

Determination of Auger decay widths with the Feshbach-Fano method

In the Feshbach-Fano method, the wave function of a core-ionized state is partitioned into a bound and a continuum part, and the decay width is obtained channel per channel from the imaginary part of the complex-valued interaction energy between the two parts.[57–59] A recent implementation of this method[65] employs a CVS-EOMIP-CCSD wave function as representation of the bound part and a product of an EOMDIP-CCSD wave function and a plane wave or a Coulomb wave for the Auger electron for each continuum state.

Using plane waves is computationally simple, but assuming that the wave function of the outgoing electron is not affected by the molecular field is a crude approximation. In contrast, a Coulomb wave captures the attractive forces between the dicationic molecular core and the Auger electron better. However, the origin of a Coulomb wave and the charge associated with it make substantial impact on the partial widths although there are not always obvious choices for these parameters when one deals with molecules.[63,66] In this work, we use plane waves even though an improvement may be achievable by placing a Coulomb wave at the center of charges.

A drawback of the Feshbach-Fano approach is that there is no direct access to the total decay width, which can be computed only as sum of partial widths. Because higher-lying EOMDIP-CCSD states often cannot be converged due to mixing with higher-order excitations, the total decay width obtained from Fano-EOM-CCSD calculations is sometimes too small compared to results from CBF calculations, in which all decay channels are by construction included. However, we recently showed that, even though the two approaches describe Auger decay in different ways, CBF-CCSD and Fano-EOM-CCSD agree well with each other about the Auger spectrum of benzene.[78]

Mapping between Auger electron energies and decay widths

Within the Fano-EOM-CCSD method, the Auger decay channels are defined in terms of EOMDIP-CCSD wave functions, which comprise $2h$ and $3h1p$ configurations. Because partial widths and Auger electron energies are determined from the same wave functions, there is no problem to assign widths to energies.

In contrast, the CBF-EOMIP-CCSD and CBF-CCSD methods yield partial widths for individual $2h$ configurations in the wave function of the core-ionized state. Additional steps are necessary to map these partial widths onto the Auger electron energies, which are obtained from separate EOMDIP-CCSD calculations.

The easiest approach is to assign each EOMDIP-CCSD state to a single $2h$ configuration

from the CBF-CCSD or CBF-EOMIP-CCSD calculation but this does not lead to convincing results.[78] Instead, a weighting procedure is necessary where each EOMDIP-CCSD state is assigned a combination of partial widths using the EOMDIP-CCSD amplitudes as weighting coefficients. This gives good results as we recently showed for the Auger spectrum of benzene.[78]

Here, we refine this approach by taking into account that the $2h$ character of the EOMDIP-CCSD states varies. Specifically, these states can have substantial contributions from $3h1p$ excitations that correspond to satellite states or do not represent Auger decay channels at all. In this work, we map the decay widths only onto the $2h$ part of every EOMDIP-CCSD state, whereas the $3h1p$ parts are assigned widths of zero. As documented in the Supporting Information, this leads to improvements in the peak intensities as compared to our previous approach.

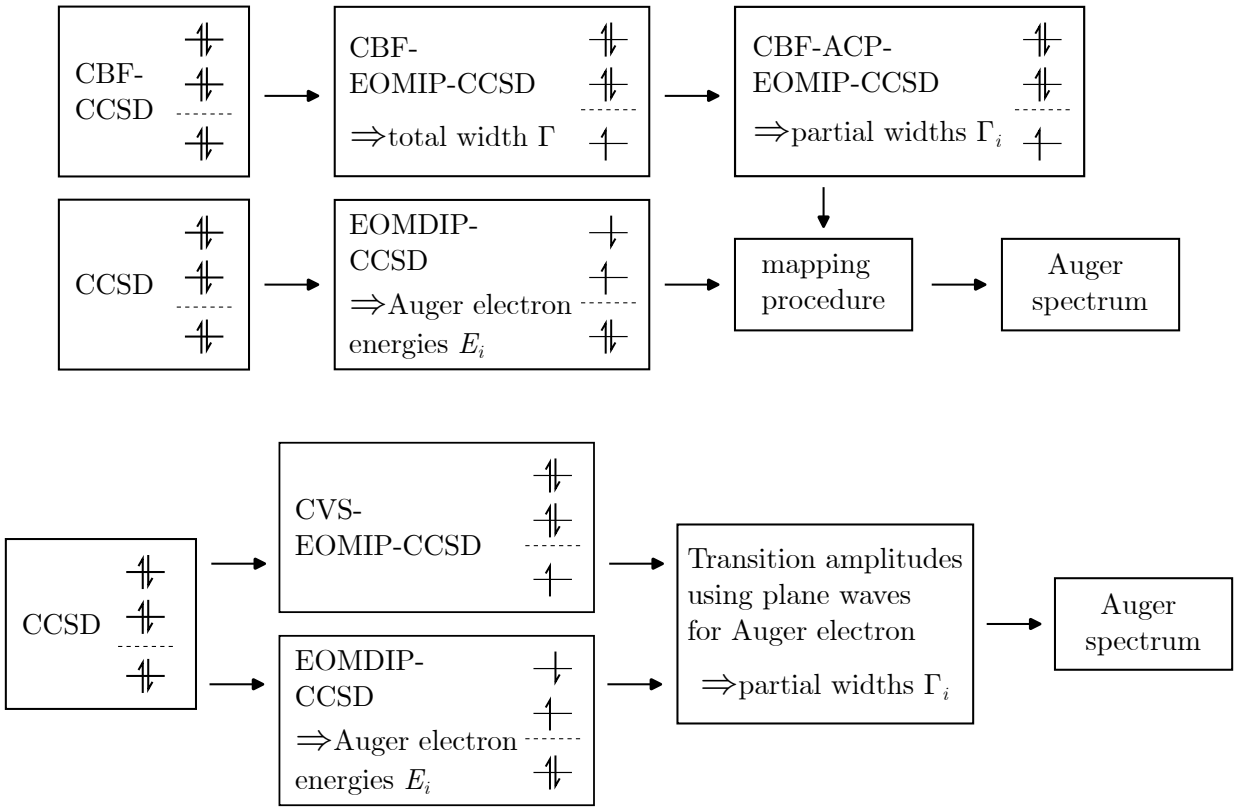

Figure 1: Flowcharts explaining different approaches for computing Auger spectra based on EOM-CC wave functions. Upper panel: Complex basis function approach. Lower panel: Feshbach-Fano approach.

Electronic structure of the studied molecules

The canonical molecular orbitals (MOs) of the investigated molecules are shown in Figure 2 and the corresponding orbital energies are available from Table 1. While methane only has one core orbital, ethane, ethylene, and acetylene have two core orbitals, one *gerade* and one *ungerade*, which are composed of the 1s orbitals of the two carbon atoms.

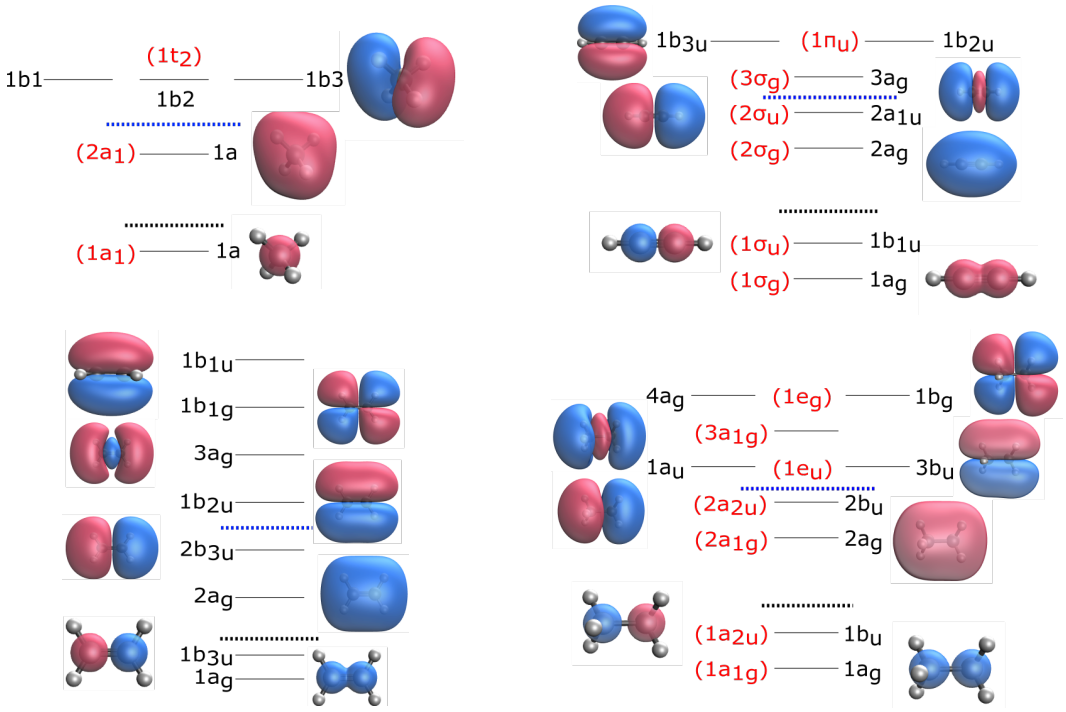

Figure 2: MO diagrams of methane, acetylene, ethylene, and ethane (from top left to bottom right). The black labels are the irreducible representations in the Abelian subgroup in which the calculation is carried out, the red labels are the irreducible representations in the full point group. Core orbitals, inner-valence orbitals, and outer-valence orbitals are separated by black and blue dashed lines.

To better compare the Auger decay channels between the molecules, we group the valence MOs in three ways: first, by inversion symmetry as *gerade* and *ungerade*; second, as C-C bonding or antibonding depending on whether there is a nodal plane between the carbon atoms; and finally, as inner valence or outer valence. Note, however, that the orbitals referred to as C-C-antibonding have C-H bonding character. The distinction between inner-valence and outer-valence orbitals is motivated by the fact that inner-valence holes decay through

Table 1: Energies in Hartree of the MOs of methane, acetylene, ethylene, and ethane. The bonding or antibonding character of the MOs with respect to the C-C bond and the designation as core, inner valence, or outer valence is given as well.

Methane			
$1a_1$		core	–11.208
$2a_1$		inner val.	–0.940
$2t_2$		outer val.	–0.544

Acetylene			
$1\sigma_g$	bonding	core	–11.245
$1\sigma_u$	antib.	core	–11.241
$2\sigma_g$	bonding	inner val.	–1.029
$2\sigma_u$	antib.	inner val.	–0.766
$3\sigma_g$	bonding	outer val.	–0.680
$1\pi_u$	bonding	outer val.	–0.410

Ethylene			
$1a_g$	bonding	core	–11.233
$1b_{3u}$	antib.	core	–11.231
$2a_g$	bonding	inner val.	–1.032
$2b_{3u}$	antib.	inner val.	–0.792
$1b_{2u}$	bonding	outer val.	–0.641
$3a_g$	bonding	outer val.	–0.589
$1b_{1g}$	antib.	outer val.	–0.506
$1b_{1u}$	bonding	outer val.	–0.377

Ethane			
$1a_{1g}$	bonding	core	–11.213
$1a_{2u}$	antib.	core	–11.213
$2a_{1g}$	bonding	inner val.	–1.014
$2a_{2u}$	antib.	inner val.	–0.840
$1e_u$	bonding	outer val.	–0.594
$3a_{1g}$	bonding	outer val.	–0.509
$1e_g$	antib.	outer val.	–0.486

different pathways than outer-valence holes. Specifically, interatomic Coulombic decay[87,88] and excess-energy controlled fragmentation[29] have been observed only for inner-valence holes. We label all MOs that are mainly composed of carbon 2s orbitals as inner valence and all higher-lying orbitals as outer valence. However, as illustrated by Table 1, there is no clear energetic separation between inner-valence and outer-valence MOs.

Computational details

All molecules were studied at their equilibrium structures as determined with B3LYP/6-311+G(3df). The molecular point groups are T_d for methane, $D_{\infty h}$ for acetylene, D_{2h} for ethylene, and D_{3d} for ethane (staggered conformation). Calculations were carried out in the largest Abelian subgroups, which are D_2 for methane, D_{2h} for acetylene and ethylene, and C_{2h} for ethane. Cartesian coordinates are available from the Supporting Information.

CBF-CCSD and CBF-EOMIP-CCSD calculations were performed using the complex-variable codes[89,90] implemented in Q-Chem 5.[91] We used modified standard basis sets with s- and p-shells taken from the cc-pCV5Z basis set and d- and f-shells from the cc-pCVTZ basis set. Results obtained with the unmodified cc-pCVTZ basis are available from the Supporting Information. While the final Auger spectra obtained with the two basis sets are very similar, total and partial decay widths differ substantially. With cc-pCVTZ some total and partial widths are inferior, which confirms our earlier findings.[76,78]

To describe the outgoing Auger electron, three complex-scaled s-, p- and d-shells were added to the carbon atoms for the evaluation of partial widths. The exponents of these shells are taken from our earlier work[76] and can be found in the Supporting Information. In the EOMDIP-CCSD calculations, no complex-scaled shells were added to the basis.

In all CBF calculations, the optimal complex-scaling angle θ_{opt} was determined by minimizing the derivative $|\mathrm{d}E/\mathrm{d}\theta|$ where E is the difference between the energy of the ground state and that of the core-ionized state.[47,76,92] This was done by recomputing the energy for θ-values between 0° and 45° in steps of 1°. Partial widths were then computed at the θ_{opt} values. For CBF-CCSD, this was done through decomposition of the imaginary energy,[76] and for CBF-EOMIP-CCSD using the ACP approach.[77]

For Fano-EOM-CCSD calculations we used the same basis sets but without complex scaling the additional shells. Plane waves were used to represent the Auger electron[65] except for methane where we also show results from Ref. 66 that were obtained using a Coulomb wave. The same number of EOMDIP-CCSD states were included in the Fano-EOM-CCSD and CBF-(EOMIP)-CCSD calculations so that the resulting Auger spectra have the same level of completeness. CVS was invoked for Fano-EOM-CCSD calculations but not for CBF-EOM-CCSD and CBF-CCSD calculations.

For acetylene, ethylene, and ethane, both core-ionized states were computed, while only one exists in methane. The number of EOMDIP-CCSD target states taken into account is 16 for methane, 25 for acetylene, 36 for ethylene, and 49 for ethane. This equates for each

molecule to the number of possible combinations of two valence spin orbitals. We note that the ACP variant of the CBF approach requires some additional calculations to determine partial widths for molecules with non-Abelian point groups.[77]

For the construction of the Auger spectra of acetylene, ethylene, and ethane, we averaged the widths computed for the *gerade* and the *ungerade* core holes. In addition to spectra based on CBF-EOMIP-CCSD and Fano-EOM-CCSD partial widths, we also constructed Auger spectra where we replaced partial widths by the density of EOMDIP-CCSD states. This equates to the assumption that every decay channel has the same width, which was previously used to compute Auger spectra with the ADC(2) method.[22,23,93]

All Auger spectra were normalized such that the intensity of the strongest peak became identical. To the resulting stick spectra, we applied a Gaussian broadening function with a full width at half maximum equal to 1.5 eV. Furthermore, for each molecule the theoretical spectra were shifted to lower Auger electron energies to align the position of the highest-energy peak with the respective experimental spectrum. The applied energy shifts amount to 0.1 eV, 2.0 eV, 2.0 eV, and 0.2 eV for the Fano-EOM-CCSD spectra of methane, acetylene, ethylene, and ethane, respectively, and to 1.2 eV, 3.0 eV, 3.1 eV, and 1.7 eV for the CBF-EOMIP-CCSD spectra of methane, acetylene, ethylene, and ethane, respectively. We note that the difference between the shifts for Fano-EOM-CCSD and CBF-EOMIP-CCSD is almost exclusively due to the use of CVS in the former calculations.

Results and discussion

Total decay widths

Our results for total decay widths are given in Table 2. Evidently, the width of the carbon 1s hole does not differ much between the molecules. This is in contrast to the strong dependence on the nuclear charge and the energy of the core-hole.[1,77,94,95] The decay widths of the *gerade* and *ungerade* core holes in ethane and ethylene are pairwise identical up to 1–2

meV, while the decay width of methane appears to be a little larger, which is in agreement with experimental results.[25,27] We note good agreement between CBF-based calculations and Fano-EOM-CCSD in Table 2. This is surprising given that Fano-EOM-CCSD only yielded ca. 55% of the CBF-CCSD total width in our recent study of the Auger spectrum of benzene.[78] We consider the good agreement as an indication that our calculations include all relevant EOMDIP-CCSD states.

Table 2: Total decay half-widths in meV of core-ionized methane, ethane, ethylene, and acetylene.

Method	Core-hole	C_2H_6	C_2H_4	C_2H_2	CH_4
CBF-EOMIP-CCSD	*gerade*	39.0	36.6	39.0	40.1
	ungerade	37.5	38.6	40.1	
CBF-ΔCCSD	*gerade*	38.0	34.4	43.0	43.4
	ungerade	36.4	37.6	43.2	
Fano-EOM-CCSD	*gerade*	40.7	38.6	41.6	46.9
	ungerade	41.6	41.4	46.6	
expt.				45 ± 5[25]	48 ± 1[27]

Partial decay widths of methane

Partial decay widths computed for methane are given in Table 3. Methane only has 8 valence electrons and, as a consequence, there are only 7 dicationic states of $2h$ character. The Auger spectrum is dominated by double ionization of the HOMO ($1t_2$); the resulting ^1E and $^1T_2$ states contribute roughly half of the total decay width. This dominance can be explained by the threefold degeneracy of the $1t_2$ orbital: Out of the 16 possible combinations of the valence orbitals of methane, 9 involve only the $1t_2$ orbital so that one would expect a share of 56% assuming equal decay widths for every channel. Other channels, however, show clear deviations from this naive expectation: The $^3T_1$ ground state of the methane dication is not produced at all and the $^3T_2$ state also has a reduced partial width. On the contrary, double ionization of the $2a_1$ inner-valence orbital is enhanced. Assuming equal widths for every channel, one would expect a contribution of 6% while our calculations deliver values of

12%. We note that the suppression of triplet channels and the enhancement of inner-valence channels are both in agreement with earlier observations.[56,77,78,96]

Table 3: Partial decay half-widths in meV of core-ionized methane. Dissociation pathways of the dicationic target states are given as well.

State	Electronic configuration	CBF-EOMIP-CCSD/ACP	CBF-CCSD /decomp.	Dissociation channel
$^1A_1$	$2a_1^{-2}$	6.0	6.7	excess-energy-determined[29]
$^1T_2$	$2a_1^{-1}1t_2^{-1}$	10.4	15.1	C^++H^++3H[21]/multiple[29]
$^3T_2$	$2a_1^{-1}1t_2^{-1}$	2.8	4.7	multiple[29]
$^1A_1$	$1t_2^{-2}$	0.9	1.6	CH^++H^++H_2[21]
$^1T_2$	$1t_2^{-2}$	11.6	15.4	CH_2^++H_2^+[21]
^1E	$1t_2^{-2}$	7.3	11.2	CH_3^++H^+[21]
$^3T_1$	$1t_2^{-2}$	0.0	0.0	–[21]

Table 3 shows relatively large deviations between CBF-EOMIP-CCSD and CBF-CCSD partial widths. This is most pronounced for the ^1E and $^1T_2$ channels where CBF-CCSD values are larger by up to 50%, while the agreement is much better for the $^1A_1$ channels. While the sum of the partial widths (39.0 meV) matches the total width (40.1 meV) well for CBF-EOMIP-CCSD, this is not the case for CBF-CCSD (54.7 meV as compared to 43.4 meV). A decision which method delivers superior results is difficult but we note that we previously observed a similar pattern for neon and for this system CBF-CCSD results agreed better with experimental partial widths.[76,77]

The fate of the doubly-ionized states of methane has been explored before. All states undergo rapid nuclear relaxation and fragmentation via one of several different pathways is most likely,[19] although a non-dissociative pathway resulting in the $^3T_1$ state and a planar molecular structure is also possible. The assignment of fragmentation pathways to different electronic states of the dication[21] has been corroborated by calculations of the dicationic potential energy surfaces.[34] An investigation of fragmentation probabilities in coincidence with Auger electron energies revealed that the fate of states with inner-valence holes is mostly determined by the excess energy of the molecule,[29] whereas the states resulting from double ionization of the HOMO correspond to specific fragmentation pathways. Our partial

widths in Table 3 suggest that the most likely fragments are CH_2^+ and C^+, while production of CH^+ is less likely. We note, however, that the channel associated with the C^+ fragment has a larger width in our calculations as compared to the experimentally determined intensity[24] as can be seen from Figure 4.

Partial decay widths of acetylene, ethylene and ethane

Partial widths for the most intense decay channels of acetylene, ethylene, and ethane are given in Table 4. Given the large number of decay channels (33 for ethane, 36 for ethylene, and 18 for acetylene) a discussion of all partial widths is not useful. Instead, we will highlight the most significant features of each molecule and draw comparisons between them. Partial widths for all decay channels are available from the Supporting Information. Notably, CBF-EOMIP-CCSD and CBF-CCSD results are more similar than for methane. The absolute values rarely differ by more than 1 meV and the trends between the channels are the same with both methods.

Some tendencies are visible in all three molecules: For example, partial widths for most channels barely differ between *gerade* and *ungerade* core holes even though there are some exceptions like the $2\sigma_g^{-2}$ channel in acetylene or the $2a_g^{-1}3a_g^{-1}$ channel in ethylene. Also, similar to methane, most channels where both electrons stem from inner-valence orbitals have enhanced decay widths. However, this enhancement is not present for the *ungerade* inner-valence orbitals ($2\sigma_u$ in acetylene, $2b_{3u}$ in ethylene, and $2a_{2u}$ in ethane), which are closer to the outer-valence orbitals in terms of energy (see Table 1). Decay channels involving these orbitals have rather low widths.

Another common feature of acetylene and ethane is that the decay channels producing the triplet ground electronic states of the dications, $^3A_{2g}$ ($1e_g^{-2}$) for ethane and $^3\Sigma_u^-$ ($1\pi_u^{-2}$) for acetylene, have zero partial widths, whereas the lowest singlet states involving the same orbitals, ^1E_g ($1e_g^{-2}$) for ethane and $^1\Delta_g$ ($1\pi_u^{-2}$) for acetylene have relatively large partial widths. In contrast, the ethylene dication has a ^1A_g singlet ground state ($1b_{1u}^{-2}$) with a

Table 4: Largest partial decay half-widths in meV of core-ionized acetylene, ethylene, and ethane. Dissociation pathways of the dicationic target states are also shown where known.

State	Electronic configuration	CBF-EOMIP-CCSD/ACP		CBF-CCSD /decomp.		Dissociation channel
		g	u	g	u	
			Acetylene			
$^1\Pi_u$	$2\sigma_g^{-1}\ 1\pi_u^{-1}$	6.2	6.7	6.2	6.8	
$^1\Delta_g$	$1\pi_u^{-2}$	6.1	6.2	5.8	6.1	
$^1\Pi_u$	$3\sigma_g^{-1}\ 1\pi_u^{-1}$	6.2	4.9	5.7	4.5	$C_2H^+ + H^+$ [31]
$^1\Sigma_u^+$	$2\sigma_g^{-1}\ 2\sigma_u^{-1}$	3.8	4.1	4.5	4.5	
$^1\Pi_g$	$2\sigma_u^{-1}\ 1\pi_u^{-1}$	3.3	3.6	3.4	3.8	2 CH^+ [31]
$^1\Sigma_g^+$	$2\sigma_g^{-2}$	3.9	2.4	3.9	2.4	
$^1\Sigma_g^+$	$2\sigma_g^{-1}\ 3\sigma_g^{-1}$	1.8	2.3	2.2	3.1	
$^1\Sigma_g^+$	$3\sigma_g^{-2}$	1.7	2.2	1.5	1.8	
$^1\Sigma_u^+$	$2\sigma_u^{-1}\ 3\sigma_g^{-1}$	1.1	1.9	1.2	1.7	
$^3\Pi_u$	$2\sigma_g^{-1}1\pi_u^{-1}$	1.3	1.6	1.3	1.7	
			Ethylene			
$^1B_{3u}$	$2a_g^{-1}\ 2b_{3u}^{-1}$	3.3	3.4	3.3	3.9	
$^1B_{1u}$	$3a_g^{-1}\ 1b_{1u}^{-1}$	2.9	2.5	2.7	2.3	2 CH_2^+
$^1B_{1u}$	$2a_g^{-1}\ 1b_{1u}^{-1}$	2.5	2.5	2.5	2.4	
^1A_g	$2a_g^{-2}$	2.3	2.6	2.5	2.8	
^1A_g	$2a_g^{-1}\ 3a_g^{-1}$	1.6	3.1	1.8	3.1	
^1A_g	$1b_{1u}^{-2}$	2.1	2.3	2.0	2.2	nondissociative
^1A_g	$3a_g^{-2}$	2.6	1.0	2.4	1.0	$C_2H_2^+ + H_2^+$
$^1B_{2u}$	$1b_{2u}^{-1}\ 3a_g^{-1}$	1.9	1.5	1.8	1.4	$C_2H_2^+ + H_2^+$
$^1B_{3g}$	$1b_{2u}^{-1}\ 1b_{1u}^{-1}$	1.6	1.7	1.7	1.8	2 CH_2^+
$^1B_{2g}$	$2b_{3u}^{-1}\ 1b_{1u}^{-1}$	1.7	1.6	1.7	1.7	$C_2H_2^+ + H_2^+$
$^1B_{3u}$	$2b_{3u}^{-1}\ 3a_g^{-1}$	1.6	1.8	1.4	1.9	
$^1B_{1g}$	$3a_g^{-1}\ 1b_{1g}^{-1}$	1.4	1.7	1.3	1.7	
			Ethane			
^1E_u	$1e_u^{-1}\ 1e_g^{-1}$	3.6	3.6	3.9	3.9	
^1E_u	$1e_u^{-1}\ 3a_{1g}^{-1}$	3.0	3.4	2.9	3.2	
^1E_g	$3a_{1g}^{-1}\ 1e_g^{-1}$	3.4	2.9	3.2	2.9	
$^1A_{2u}$	$2a_{1g}^{-1}\ 2a_{2u}^{-1}$	3.1	2.8	3.4	3.1	
$^1A_{1g}$	$3a_{1g}^{-2}$	2.6	1.6	2.3	1.4	
^1E_g	$2a_{1g}^{-1}\ 1e_g^{-1}$	1.9	2.0	2.2	2.3	
^1E_u	$2a_{1g}^{-1}\ 1e_u^{-1}$	2.0	1.9	2.2	2.2	
$^1A_{1g}$	$2a_{1g}^{-1}\ 3a_{1g}^{-1}$	1.9	1.9	1.8	1.8	
^1E_g	$1e_u^{-2}$	1.9	1.8	1.9	1.9	
$^1A_{1g}$	$2a_{1g}^{-2}$	1.6	2.0	1.7	2.2	
^1E_g	$1e_g^{-2}$	1.8	1.8	1.9	2.0	
$^1A_{2u}$	$2a_{2u}^{-1}\ 3a_{1g}^{-1}$	2.1	1.2	1.9	1.3	

non-zero width, while the lowest triplet state ^3A_u ($1b_{1g}^{-1}1b_{1u}^{-1}$) has zero width.

In ethane, the decay channels involving the $1e_g$ and $1e_u$ orbitals display an interesting pattern. These orbitals are ca. 0.1 a.u. apart in energy, mainly describe the C-H bonds, and differ by a nodal plane perpendicular to the C-C bond. The partial widths of the respective channels are, however, almost equal meaning that an interchange of the $1e_g$ and $1e_u$ orbitals would not affect the Auger spectrum.

Previous calculations and coincidence measurements for ethylene and acetylene showed that some higher-energy decay channels lead to fragmentation pathways that produce two cations.[30,31,37,97] On the contrary, only double ionization of the HOMO does not result in dissociation. For ethylene, our calculations predict that a share of 5-6 % of molecules undergoing Auger decay do not to dissociate, which is consistent with the experimental result of 5%.[37] One can thus assume that all other decay channels lead to some sort of fragmentation.

Other results of our calculations on ethylene disagree with experimental fragmentation statistics. Only a few channels with low partial widths have been assigned to pathways involving deprotonation, while four channels are related to the production of H_2^+ according to measurements.[37] Our calculations assign substantial partial widths to these channels whereas only 2 % of the ethylene molecules follow this pathway according to experimental findings. There are several possible explanations for these inconsistencies as the one-to-one assignment of decay channels to fragmentation pathways is a simplification. For example, non-Born-Oppenheimer dynamics might need to be taken into account to model some fragmentation pathways correctly. Furthermore, other cations could fragment to form H^+, there could be unidentified fragmentation pathways of other dicationic states or excess-energy-determined fragmentation could result in deprotonation similar to methane.

Analysis of partial widths in terms of orbital characters

In order to compare acetylene, ethylene, and ethane, we classified the decay channels in four different ways and analyzed the distribution of partial widths among these categories: 1)

singlet and triplet channels; 2) channels involving two *gerade* orbitals, two *ungerade* orbitals, or one each; 3) channels involving two outer-valence orbitals, two inner-valence orbitals, or one each; 4) channels involving two C-C-bonding orbitals, two C-C-antibonding orbitals, or one each.

All results are given in Figure 3; values for the *gerade* and the *ungerade* core hole are averaged. For each category, we show the computed CBF-EOMIP-CCSD/ACP values as well as results obtained under the assumption that every decay channel has the same partial width. Fano-EOM-CCSD results are only given for singlet and triplet decay channels as well as for decay channels made up of one *gerade* and one *ungerade* orbital. The other categories are not applicable to Fano-EOM-CCSD, because here the decay channels are not defined in terms of orbital pairs but in terms of EOMDIP-CCSD states, where different orbitals can mix.

In agreement with our previous work[77] and with results for methane (see Table 3), we observe an enhancement of decay channels involving two inner-valence orbitals for all three molecules in Figure 3 (upper left panel) with respect to the assumption that all channels have the same width. Interestingly, the contribution of these decay channels does not vary much among acetylene, ethylene, and ethane and is thus almost unaffected by the number of outer-valence orbitals present.

As concerns *gerade* and *ungerade* orbitals (upper right panel of Figure 3), we only find small deviations from the results obtained under the assumption of equal decay widths for each channel. Decay channels made up of two *gerade* orbitals are somewhat enhanced while those involving two *ungerade* orbitals are somewhat suppressed.

The comparison of C-C bonding and antibonding orbitals (lower left panel of Figure 3) shows that decay channels involving two bonding orbitals are slightly enhanced with respect to the assumption of equal widths, whereas decay channels involving one bonding and one antibonding orbital are slightly suppressed. This effect is more pronounced for acetylene and ethylene than for ethane and should be viewed in relation to fragmentation induced

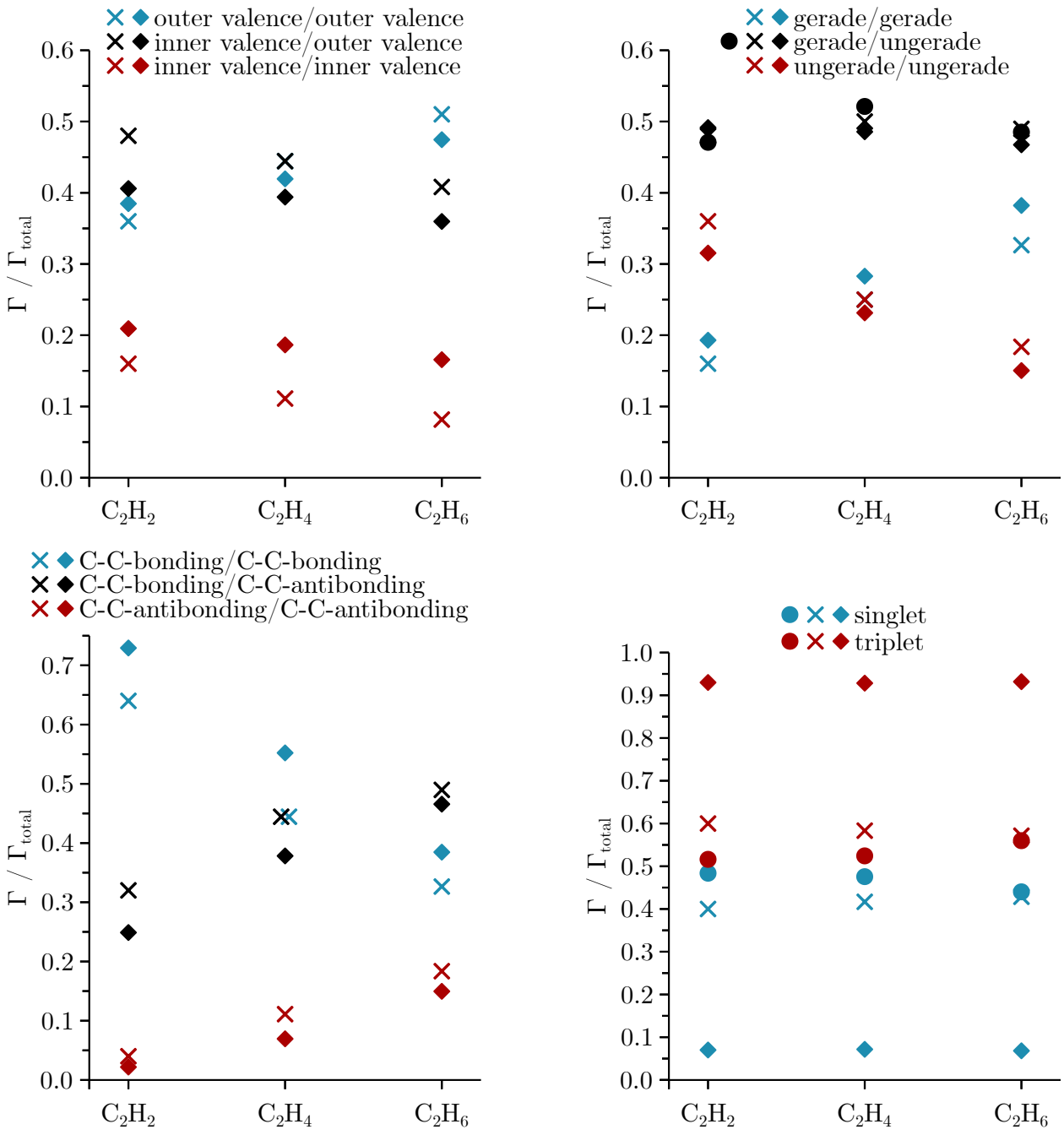

Figure 3: Relative intensities of Auger decay channels involving different orbital categories. ♦ denotes CBF-EOMIP-CCSD/ACP results, • denotes Fano-EOM-CCSD results, and × denotes results assuming equal partial widths for every channel.

by Auger decay. Although most dicationic states will undergo Coulomb explosion, one may assume that the C-C bond is especially prone to cleavage when electrons are taken from C-C bonding orbitals.

The lower right panel of Figure 3 illustrates that triplet channels have substantially smaller widths than singlet channels. CBF-EOMIP-CCSD yields a share of 91–94% for singlet channels, while only 6–9% of intensity are assigned to triplet channels. This is a well-known property of Auger decay, which has previously been analyzed in detail.[56,62,78,96,98] However, the Fano-EOM-CCSD method fails to describe the suppression of triplet channels and yields results as if all channels had the same partial widths. Similar shortcomings were observed before and are likely due to the description of the Auger electron by a plane wave.[66,78]

Auger spectra

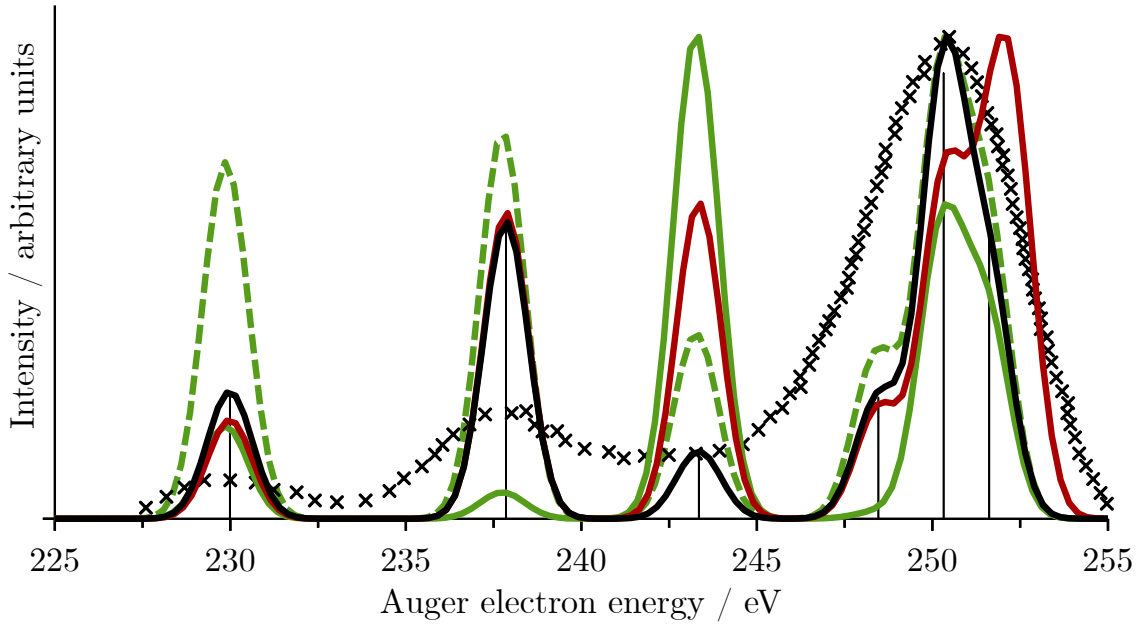

Figure 4: Auger spectrum of methane, computed with CBF-EOMIP-CCSD/ACP (black line and stick spectrum), Fano-EOM-CCSD with a plane wave (green solid line) and a Coulomb wave (green dashed line) for the outgoing electron, and assuming equal partial widths for all decay channels (red line). The experimental Auger spectrum measured by Kivimäki et al.[24] (×) is shown as well.

The Auger spectrum of methane is shown in Figure 4. This spectrum has been measured twice;[16,24] the experimental spectra overall are in good agreement with each other but the first experiment identified four peaks, while the second experiment found only three peaks. Our calculations reveal that the highest-energy peak at around 247–253 eV comprises contributions from three dicationic states (^{1}E, ^{1}T$_2$, ^{1}A$_1$) that all result from double ionization of the HOMO, whereas the other peaks correspond to one decay channel each. The ^{3}T$_2$ state, which represents the only active triplet decay channel, is only visible in one of the experimental spectra. Our theoretical spectra differ substantially from each other and none of them agrees with the experimental spectra about all peaks. When assuming equal partial widths, the intensities of the peaks at 243 eV (^{3}T$_2$, 2a^{-1}1t$_2^{-1}$) and 237 eV (^{1}T$_2$, 2a^{-1}1t$_2^{-1}$) are significantly overestimated. With Fano-EOM-CCSD, the intensity of the ^{3}T$_2$ channel at 243 eV is overestimated when using plane waves, whereas with Coulomb waves the peaks at 237 eV and 230 eV are too intense compared to experiment. CBF-EOMIP-CCSD also assigns more intensity to the peak at 237 eV than it has in the experimental spectrum but captures the overall distribution of intensity relatively well.

The Auger spectrum of acetylene is displayed in Figure 5. Consistent with the lower double-ionization threshold of acetylene as compared to methane, the onset of the Auger spectrum is at higher Auger electron energies. The experimental spectrum[16] comprises one very broad peak and two narrower ones. Our calculations indicate that each peak is made up of multiple decay channels. The highest-energy peak at around 256 eV corresponds to decay into the $^1\Delta_g$ and $^1\Sigma_g^+$ states, both of which arise from double ionization of the HOMO ($1\pi_u$). The second peak at around 250 eV mainly comprises contributions from two states, $^1\Pi_u$ and $^1\Pi_g$, that arise from ionization of HOMO and HOMO–1 as well as HOMO and HOMO–2, respectively. The broad peak between 246 and 232 eV is made up of six singlet and four triplet channels. According to our calculations, there should be one more peak at around 224 eV corresponding to double ionization of the innermost valence orbital ($2\sigma_g$) but this peak is absent from the experimental spectrum.

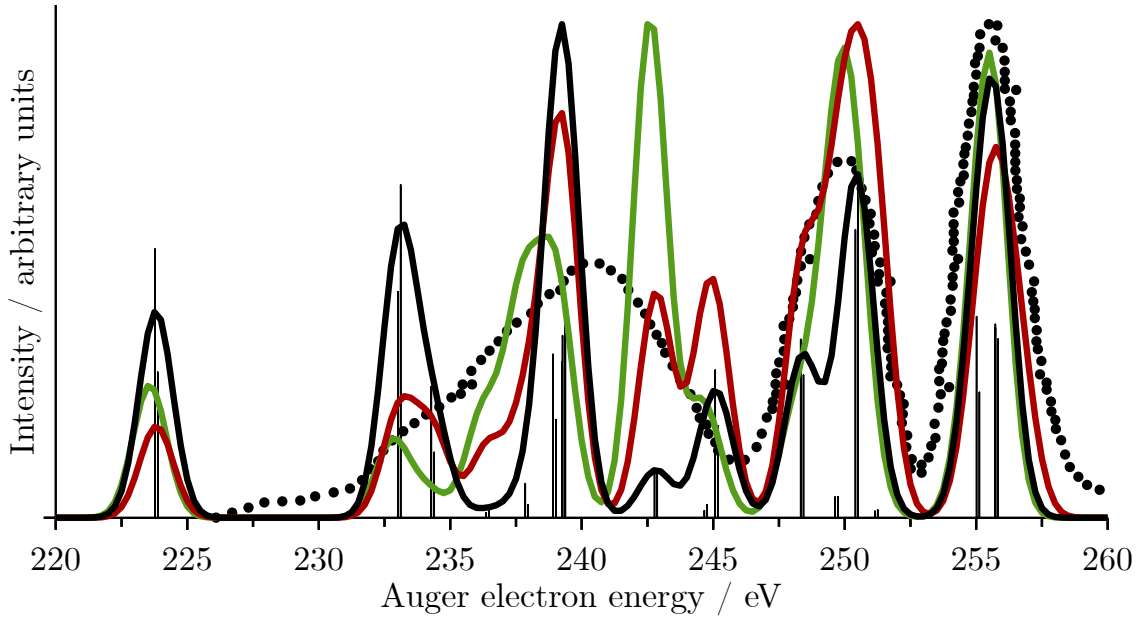

Figure 5: Auger spectrum of acetylene, computed with CBF-EOMIP-CCSD/ACP (black line and stick spectrum), Fano-EOM-CCSD with a plane wave for the outgoing electron (green line), and assuming equal partial widths for all decay channels (red line). The experimental Auger spectrum[16] is shown as black dotted line.

In agreement with experiment, the peak at 256 eV is more intense than the one at 250 eV in the CBF-EOMIP-CCSD spectrum, whereas Fano-EOM-CCSD predicts equal intensities and the assumption of equal widths for each channel even leads to an inverted pattern with the lower-energy peak being more intense. On the contrary, earlier theoretical results based on a Green's function method[20] arrived at a too low relative intensity of the peak at 250 eV as shown in the Supporting information. Below 246 eV, the agreement among the spectra is considerably less good, a likely reason being broadening due to vibrational interference,[32,99,100] which is not included in our theoretical modeling. The best agreement with experiment is observed for CBF-EOMIP-CCSD, where we obtain one dominant peak at 239 eV and weaker signals at 224 eV, 233 eV, 243 eV, and 245 eV. Similar signals are also present in the earlier theoretical spectrum,[20] but have a much lower intensity than in our CBF-EOMIP-CCSD spectrum. In contrast, Fano-EOM-CCSD overestimates the intensity of the $^3\Pi_u$ and $^3\Pi_g$ states, resulting in a prominent peak at 243 eV, which is absent from the experimental spectrum.

Finally, we note that the experimental spectrum has a shoulder at the high-energy end at around 260 eV that is not present in any theoretical spectrum. This may possibly be caused by nuclear motion.

The Auger spectrum of ethylene is displayed in Figure 6. The experimental spectrum[16] has six peaks and, by and large, is in good agreement with our results. All theoretical approaches yield eight peaks but their positions agree well with experiment and it looks as if two peaks are simply not resolved in the experimental spectrum, which may be due to dissociation. Notably, the decay channels with the lowest energy at around 232 eV are present in the experimental spectrum of ethylene as opposed to that of acetylene. We note that earlier theoretical results[20] shown in the Supporting Information suggested a continuation of the spectrum down to an Auger electron energy of only 224 eV, which is neither observed in experiments nor in our computations.

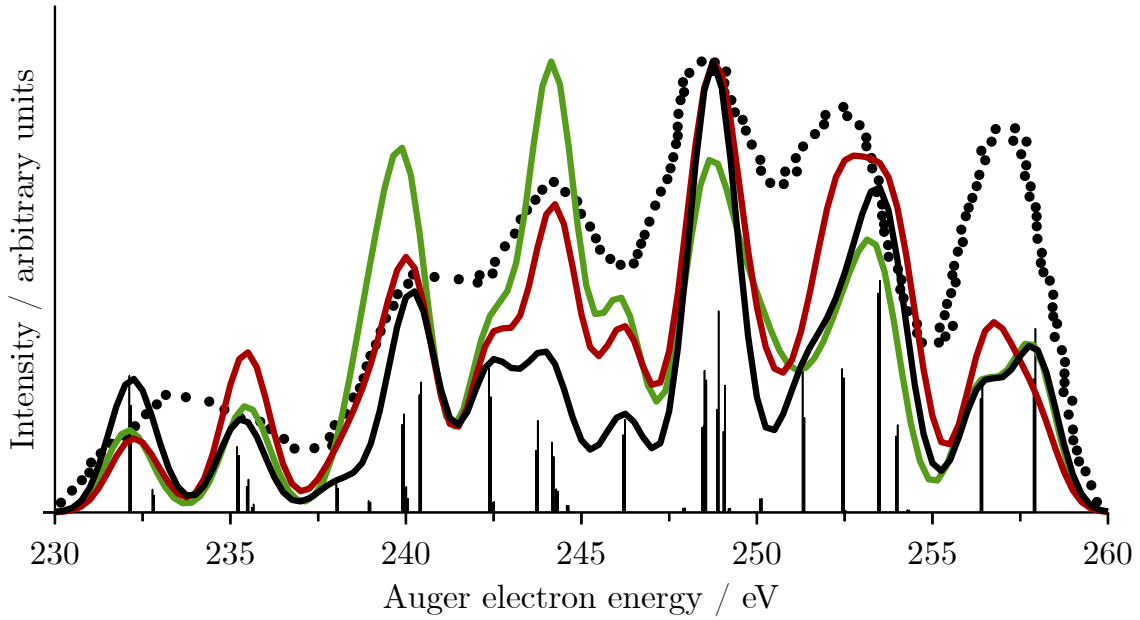

Figure 6: Auger spectrum of ethylene, computed with CBF-EOMIP-CCSD/ACP (black line and stick spectrum), Fano-EOM-CCSD with a plane wave for the outgoing electron (green line), and assuming equal partial widths for all decay channels (red line). The experimental Auger spectrum[16] is shown as black dotted line.

While most peaks are made up of many decay channels, the highest-energy peak at around 257 eV only comprises contributions from two decay channels, $1b_{1u}^{-2}$ (HOMO/HOMO) and

$1b_{1u}^{-1}1b_{1g}^{-1}$ (HOMO/HOMO–1). Its intensity relative to experiment is underestimated by all of our methods alike, which is remarkable given that the intensity of most other peaks is reproduced better. The reasons for this mismatch remain unclear but we note that the earlier Green's function-based study[20] is well in line with experiment about the intensity of this peak. A prominent discrepancy between the methods occurs for the peak at 244 eV, which is too intense in the Fano-EOM-CCSD spectrum due to the overestimation of triplet decay widths ($2a_g^{-1}1b_{1u}^{-1}$ and $2b_{3u}^{-1}1b_{2u}^{-1}$ channels).

The Auger spectrum of ethane is shown in Figure 7. The experimental spectrum of this molecule is less well resolved than the ones discussed before, possibly due to vibrational interference, and one only can discern four to five peaks. Overall, CBF-EOMIP-CCSD shows the best agreement with the measured intensity distribution, whereas Fano-EOM-CCSD produces a prominent peak at 243 eV that is absent from the experimental spectrum and the assumption of equal widths assigns to much intensity to the high-energy end of the spectrum. The shallow peak at 237 eV, which is relatively well separated from the rest of the spectrum, comprises contributions from five singlet channels and one triplet channel according to our calculations, whereas the broad feature between 243 eV and 257 eV represents all other 27 decay channels. A similar result regarding the relative intensity of the two main structures was obtained by an earlier theoretical study based on Hartree-Fock theory,[17] which is compared to our results in the Supporting Information.

Conclusions

We presented partial Auger decay widths for core-ionized methane, acetylene, ethylene, and ethane computed with the method of complex basis functions and the Feshbach-Fano approach, both combined with EOM-CCSD. From these results, we constructed theoretical Auger spectra for the four molecules and compared them to experimental spectra and previous theoretical results.

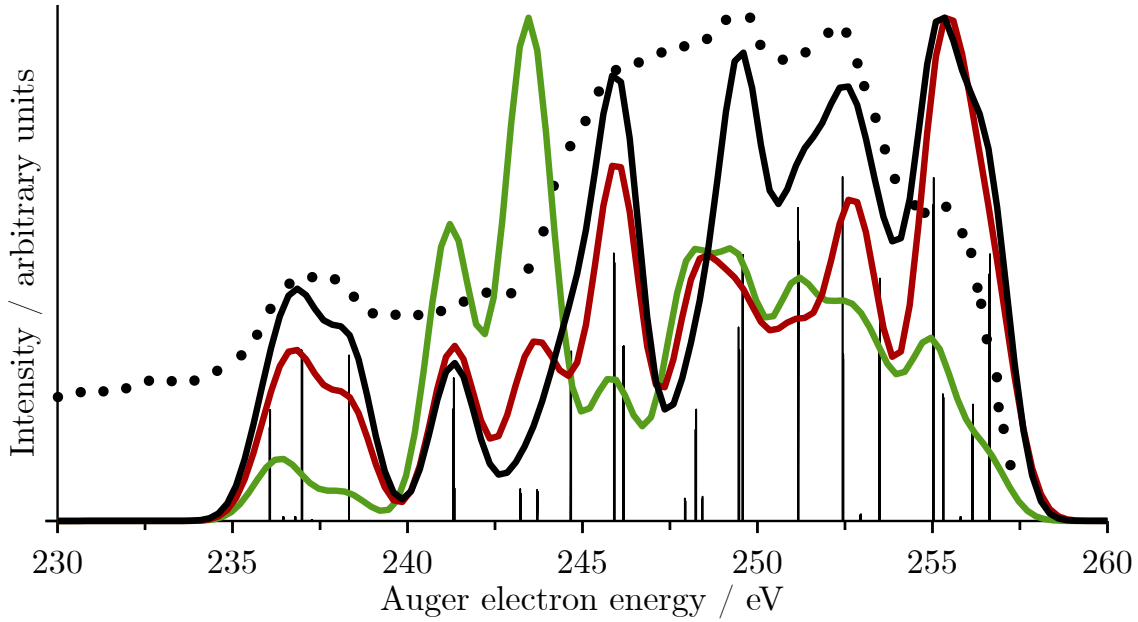

Figure 7: Auger spectrum of ethane, computed with CBF-EOMIP-CCSD/ACP (black line and stick spectrum), Fano-EOM-CCSD with a plane wave for the outgoing electron (green line), and assuming equal partial widths for all decay channels (red line). The experimental Auger spectrum[17] is shown as black dotted line.

We analyzed the intensity distribution among the Auger decay channels in four different ways: 1) singlet vs. triplet channels, 2) inner-valence vs. outer-valence orbitals, 3) *gerade* vs. *ungerade* orbitals, and 4) C-C bonding vs. C-C antibonding orbitals. In agreement with previous investigations, we found that K-shell Auger spectra are dominated by singlet channels, while triplet channels are suppressed. Also, decay channels involving inner-valence orbitals are enhanced. In contrast, inversion symmetry and the bonding or antibonding character of an orbital do not make a significant impact on Auger intensities.

Our results show that some features of Auger spectra can already be explained by assuming equal intensities for all decay channels. This approach may, however, lead to substantial misassessment of intensities, most obviously due to overestimating the contribution of triplet channels. The explicit calculation of partial decay widths clearly yields improved Auger spectra even though we observed substantial discrepancies with the experimental spectra for most molecules. This may be caused by effects that are neglected in our computations such as resonant Auger decay, shake-up processes and vibrational interferences.

The two theoretical approaches that we used for the computation of partial decay widths feature different strengths and weaknesses: On the one hand, Fano-EOM-CCSD is computationally less expensive because there is no need for complex algebra in the electronic-structure calculations. Also, no special procedure is required to assign widths to energies because both quantities are computed in the same calculations. A major problem is, however, the use of plane waves in Fano-EOM-CCSD calculations, which can lead to significant artifacts, especially too high intensities for triplet decay channels. On the other hand, CBF-EOMIP-CCSD and CBF-CCSD offer direct access to total decay widths, which are not easily accessibly in a Fano-EOM-CCSD treatment. Moreover, CBF methods do not require any assumption about the wave function of the Auger electron yielding a more realistic distribution of intensity between singlet and triplet decay channels.

Acknowledgement

We thank Dr. Wojciech Skomorowski for support regarding the Fano-EOM-CCSD code in Q-Chem, as well as Anthuan Ferino-Pérez for helpful discussions about different methods to generate Auger spectra. Furthermore, we thank Dr. Michiel van Setten for comments about how to establish the comparison to experimental results. T.-C. J. gratefully acknowledges funding from the European Research Council (ERC) under the European Union's Horizon 2020 research and innovation program (Grant Agreement No. 851766), from the KU Leuven internal funds (Grant C14/22/083) and from the Central Europe Leuven Strategic Alliance (Grant 22/014). F. M. is grateful for a Kekulé fellowship (Grant No. K 208/24) by the Fonds der Chemischen Industrie.

Supporting Information Available

The following files are available free of charge.

- Auger-decay-methane-acetylene-ethylene-ethane-SI.pdf: Cartesian coordinates of all studied molecules. Exponents of basis functions used in this work. Complete lists of all decay widths, computed for all molecules with different mapping methods and two different basis sets. Auger spectra computed with the cc-pCVTZ basis set and in comparison to earlier theoretical studies. Auger spectrum computed with a different weighting method.

References

(1) Agarwal, B. K. *X-ray spectroscopy: An introduction*; Springer, 2013.

(2) Kraus, P. M.; Zürch, M.; Cushing, S. K.; Neumark, D. M.; Leone, S. R. The ultrafast X-ray spectroscopy revolution in chemical dynamics. *Nat. Rev. Chem.* **2018**, *2*, 82.

(3) Rye, R. R.; Houston, J. E. Molecular Auger spectroscopy. *Accounts Chem. Res.* **1984**, *17*, 41.

(4) Bolognesi, P.; O'Keeffe, P.; Ovcharenko, Y.; Avaldi, L.; Carravetta, V. Resonant Auger spectroscopy at the carbon and nitrogen K-edges of pyrimidine. *J. Chem. Phys.* **2012**, *136*, 154308.

(5) Hofmann, S. *Auger- and X-ray photoelectron spectroscopy in materials science: A user-oriented guide*; Springer Science & Business Media, 2012; Vol. 49.

(6) McFarland, B. K.; Farrell, J. P.; Miyabe, S.; Tarantelli, F.; Aguilar, A.; Berrah, N.; Bostedt, C.; Bozek, J. D.; Bucksbaum, P. H.; Castagna, J. C. et al. Ultrafast X-ray Auger probing of photoexcited molecular dynamics. *Nat. Commun.* **2014**, *5*, 4235.

(7) Marchenko, T.; Inhester, L.; Goldsztejn, G.; Travnikova, O.; Journel, L.; Guillemin, R.; Ismail, I.; Koulentianos, D.; Céolin, D.; Püttner, R. et al. Ultrafast nuclear dynamics

in the doubly-core-ionized water molecule observed via Auger spectroscopy. *Phys. Rev. A* **2018**, *98*, 063403.

(8) Plekan, O.; Sa'adeh, A., H.and Ciavardini; Callegari, C.; Cautero, G.; Dri, C.; Di Fraia, M.; Prince, K. C.; Richter, R.; Sergo, R.; Stebel, L. et al. Experimental and theoretical photoemission study of indole and its derivatives in the gas phase. *J. Phys. Chem. A* **2020**, *124*, 4115.

(9) Meitner, L. Über die β-Strahl-Spektra und ihren Zusammenhang mit der γ-Strahlung. *Z. Phys.* **1922**, *11*, 35.

(10) Auger, P. Sur les rayons β secondaires produits dans un gaz par des rayons X. *CR Acad. Sci. (F)* **1923**, *177*, 169.

(11) Bambynek, W.; Crasemann, B.; Fink, R. W.; Freund, H.-U.; Mark, H.; Swift, C. D.; Price, R. E.; Rao, P. V. X-Ray fluorescence yields, Auger, and Coster-Kronig transition probabilities. *Rev. Mod. Phys.* **1972**, *44*, 716.

(12) Thompson, A. C.; Vaughan, D.; Kirz, J.; Attwood, D. E.; Gullikson, E. M.; Howells, M. R.; Kim, K.-J.; Kortright, J. B.; Lindau, I.; Pianetta, P. et al. *X-ray data booklet*; Lawrence Berkeley National Laboratory, 2009.

(13) Brown, G. S.; Chen, M. H.; Crasemann, B.; Ice, G. E. Observation of the Auger resonant Raman effect. *Phys. Rev. Lett.* **1980**, *45*, 1937.

(14) Armen, B. G.; Aksela, H.; Åberg, T.; Aksela, S. The resonant Auger effect. *J. Phys. B–At. Mol. Opt.* **2000**, *33*, R49.

(15) Carlson, T. A.; Krause, M. O. Experimental evidence for double electron emission in an Auger process. *Phys. Rev. Lett.* **1965**, *14*, 390.

(16) Rye, R. R.; Madey, T. E.; Houston, J. E.; Holloway, P. H. Chemical-state effects in Auger electron spectroscopy. *J. Chem. Phys.* **1978**, *69*, 1504.

(17) Rye, R. R.; Jennison, D. R.; Houston, J. E. Auger spectra of alkanes. *J. Chem. Phys.* **1980**, *73*, 4867.

(18) Kvalheim, O. M. Final state correlation effects on the Auger transition rates of methane. *Chem. Phys. Lett.* **1982**, *86*, 159.

(19) Siegbahn, P. E. M. Double ionization of methane. *Chem. Phys.* **1982**, *66*, 443.

(20) Liegener, C.-M. Calculations on the auger spectra of ethylene and acetylene. *Chem. Phys.* **1985**, *92*, 97.

(21) Hatherly, P. A.; Stankiewicz, M.; Frasinski, L. J.; Codling, K.; MacDonald, M. A. Double photoionisation of methane studied by the triple coincidence (PEPIPICO) technique. *Chem. Phys. Lett.* **1989**, *159*, 355.

(22) Ohrendorf, E.; Koeppel, H.; Cederbaum, L. S.; Tarantelli, F.; Sgamellotti, A. On the Auger spectrum of ethylene. *J. Electron Spectrosc.* **1990**, *51*, 211.

(23) Ohrendorf, E. M.; Tarantelli, F.; Cederbaum, L. S. Dicationic states of hydrocarbons and a statistical approach to their Auger spectra. *J. Chem. Phys.* **1990**, *92*, 2984.

(24) Kivimäki, A.; Neeb, M.; Kempgens, B.; Köppe, H. M.; Bradshaw, A. M. The C 1s Auger decay spectrum of the CH_4 molecule: The effects of vibrational fine structure, double excitations and shake-up transitions. *J. Phys. B–At. Mol. Opt.* **1996**, *29*, 2701.

(25) Kempgens, B.; Köppel, H.; Kivimäki, A.; Neeb, M.; Cederbaum, L. S.; Bradshaw, A. M. Core level energy splitting in the C 1s photoelectron spectrum of C_2H_2. *Phys. Rev. Lett.* **1997**, *79*, 3617.

(26) Kivimäki, A.; Neeb, M.; Kempgens, B.; Köppe, H. M.; Maier, K.; Bradshaw, A. M. Angle-resolved Auger spectra of the C_2H_2 molecule. *J. Phys. B–At. Mol. Opt.* **1997**, *30*, 4279.

(27) Carroll, T. X.; Berrah, N.; Bozek, J.; Hahne, J.; Kukk, E.; Sæthre, L. J.; Thomas, T. D. Carbon 1*s* photoelectron spectrum of methane: Vibrational excitation and core-hole lifetime. *Phys. Rev. A* **1999**, *59*, 3386.

(28) Rennie, E. E.; Köppe, H. M.; Kempgens, B.; Hergenhahn, U.; Kivimäki, A.; Maier, K.; Neeb, M.; Rüdel, A.; Bradshaw, A. M. Vibrational and shake-up excitations in the C 1s photoionization of ethane and deuterated ethane. *J. Phys. B–At. Mol. Opt.* **1999**, *32*, 2691.

(29) Kukk, E.; Prümper, G.; Sankari, R.; Hoshino, M.; Makochekanwa, C.; Kitajima, M.; Tanaka, H.; Yoshida, H.; Tamenori, Y.; Rachlew, E. et al. Electronic state dependence in the dissociation of core-ionized methane. *J. Phys. B–At. Mol. Opt.* **2007**, *40*, 3677.

(30) Flammini, R.; Fainelli, E.; Maracci, F.; Avaldi, L. Vinylidene dissociation following the Auger-electron decay of inner-shell ionized acetylene. *Phys. Rev. A* **2008**, *77*, 044701.

(31) Osipov, T.; Rescigno, T. N.; Weber, T.; Miyabe, S.; Jahnke, T.; Alnaser, A. S.; Hertlein, M. P.; Jagutzki, O.; Schmidt, L. P. H.; Schöffler, M. et al. Fragmentation pathways for selected electronic states of the acetylene dication. *J. Phys. B–At. Mol. Opt.* **2008**, *41*, 091001.

(32) Liu, J.-C.; Nicolas, C.; Sun, Y.-P.; Flammini, R.; O'Keeffe, P.; Avaldi, L.; Morin, P.; Kimberg, V.; Kosugi, N.; Gel'mukhanov, F. et al. Multimode resonant Auger scattering from the ethene molecule. *J. Phys. Chem. B* **2011**, *115*, 5103.

(33) Flammini, R.; Satta, M.; Fainelli, E.; Avaldi, L. A study of selected fragmentation paths of the ethyne dication: Theory and experiment. *Phys. Chem. Chem. Phys.* **2011**, *13*, 19607.

(34) Williams, J. B.; Trevisan, C. S.; Schöffler, M. S.; Jahnke, T.; Bocharova, I.; Kim, H.; Ulrich, B.; Wallauer, R.; Sturm, F.; Rescigno, T. N. et al. Probing the dynamics of

dissociation of methane following core ionization using three-dimensional molecular-frame photoelectron angular distributions. *J. Phys. B–At. Mol. Opt.* **2012**, *45*, 194003.

(35) Wolff, W.; Sigaud, L.; Montenegro, E. C.; de Jesus, V. L. B.; Cavasso Filho, R. L.; Pilling, S.; Santos, A. C. F. Ionization and fragmentation of Methane induced by 40 eV to 480 eV synchrotron radiation: From valence to beyond core electron ionization. *J. Phys. Chem. A* **2013**, *117*, 56.

(36) Flammini, R.; Satta, M.; O'Keeffe, P.; Coreno, M.; Kivimäki, A.; de Simone, M.; Carbone, M.; Feyer, V.; Prince, K. C.; Avaldi, L. An experimental and theoretical study of the resonant Auger spectrum of the ethene molecule. *New J. Phys.* **2014**, *16*, 073022.

(37) Gaire, B.; Haxton, D. J.; Sturm, F. P.; Williams, J.; Gatton, A.; Bocharova, I.; Gehrken, N.; Schöffler, M.; Gassert, H.; Zeller, S. et al. Auger decay and subsequent fragmentation pathways of ethylene following K-shell ionization. *Phys. Rev. A* **2015**, *92*, 013408.

(38) Liekhus-Schmaltz, E. C.; Tenney, I.; Osipov, T.; Sanchez-Gonzalez, A.; Berrah, N.; Boll, R.; Bomme, C.; Bostedt, C.; Bozek, J. D.; Carron, S. et al. Ultrafast isomerization initiated by X-ray core ionization. *Nat. Commun.* **2015**, *6*, 8199.

(39) Menssen, A.; Trevisan, C. S.; Schöffler, M. S.; Jahnke, T.; Bocharova, I.; Sturm, F.; Gehrken, N.; Gaire, B.; Gassert, H.; Zeller, S. et al. Molecular frame photoelectron angular distributions for core ionization of ethane, carbon tetrafluoride and 1,1-difluoroethylene. *J. Phys. B–At. Mol. Opt.* **2016**, *49*, 055203.

(40) Li, Z.; Inhester, L.; Liekhus-Schmaltz, C.; Curchod, B. F. E.; Snyder Jr., J. W.; Medvedev, N.; Cryan, J.; Osipov, T.; Pabst, S.; Vendrell, O. et al. Ultrafast isomerization in acetylene dication after carbon K-shell ionization. *Nat. Commun.* **2017**, *8*, 453.

(41) Ghosh, A.; Vaval, N.; Pal, S. Auger decay rates of core hole states using equation of motion coupled cluster method. *Chem. Phys.* **2017**, *482*, 160–164.

(42) Grell, G.; Bokarev, S. I. Multi-reference protocol for (auto)ionization spectra: Application to molecules. *J. Chem. Phys.* **2020**, *152*.

(43) Gerlach, M.; Preitschopf, T.; Karaev, E.; Quitián-Lara, H. M.; Mayer, D.; Bozek, J.; Fischer, I.; F., F. R. Auger electron spectroscopy of fulminic acid, HCNO: An experimental and theoretical study. *Phys. Chem. Chem. Phys.* **2022**, *24*, 15217.

(44) Tenorio, B. N. C.; Voß, T. A.; Bokarev, S. I.; Decleva, P.; Coriani, S. Multireference approach to normal and resonant Auger spectra based on the one-center approximation. *J. Chem. Theory Comput.* **2022**, *18*, 4387.

(45) Ridente, E.; Hait, D.; Haugen, E. A.; Ross, A. D.; Neumark, D. M.; Head-Gordon, M.; Leone, S. R. Femtosecond symmetry breaking and coherent relaxation of methane cations at the carbon K-edge. **2022**, available from `https://arxiv.org/abs/2212.12875`.

(46) Moiseyev, N. *Non-Hermitian quantum mechanics*; Cambridge University Press, 2011.

(47) Jagau, T.-C. Theory of electronic resonances: Fundamental aspects and recent advances. *Chem. Commun.* **2022**, *58*, 5205–5224.

(48) Cederbaum, L. S.; Domcke, W.; Schirmer, J. Many-body theory of core holes. *Phys. Rev. A* **1980**, *22*, 206.

(49) Coriani, S.; Koch, H. Communication: X-ray absorption spectra and core-ionization potentials within a core-valence separated coupled cluster framework. *J. Chem. Phys.* **2015**, *143*, 181103.

(50) Bari, S.; Inhester, L.; Schubert, K.; Mertens, K.; Schunck, J. O.; Dörner, S.; Deinert, S.; Schwob, L.; Schippers, S.; Müller, A. et al. Inner-shell X-ray absorption spectra of the cationic series NH_y^+ (y = 0–3). *Phys. Chem. Chem. Phys.* **2019**, *21*, 16505.

(51) Frati, F.; de Groot, F.; Cerezo, J.; Santoro, F.; Cheng, L.; Faber, R.; Coriani, S. Coupled cluster study of the x-ray absorption spectra of formaldehyde derivatives at the oxygen, carbon, and fluorine K-edges. *J. Chem. Phys.* **2019**, *151*, 064107.

(52) Vidal, M. L.; Feng, X.; Epifanovsky, E.; Krylov, A. I.; Coriani, S. New and efficient equation-of-motion coupled-cluster framework for core-excited and core-ionized states. *J. Chem. Theory Comput.* **2019**, *15*, 3117.

(53) Nanda, K. D.; Vidal, M. L.; Faber, R.; Coriani, S.; Krylov, A. I. How to stay out of trouble in RIXS calculations within equation-of-motion coupled-cluster damped response theory? Safe hitchhiking in the excitation manifold by means of core–valence separation. *Phys. Chem. Chem. Phys.* **2020**, *22*, 2629.

(54) Fransson, T.; Brumboiu, I. E.; Vidal, M. L.; Norman, P.; Coriani, S.; Dreuw, A. XABOOM: An X-ray absorption benchmark of organic molecules based on carbon, nitrogen, and oxygen 1s $\rightarrow \pi^*$ transitions. *J. Chem. Theory Comput.* **2021**, *17*, 1618.

(55) Wentzel, G. Über strahlungslose Quantensprünge. *Z. Phys.* **1927**, *43*, 524.

(56) Manne, R.; Ågren, H. Auger transition amplitudes from general many-electron wavefunctions. *Chem. Phys.* **1985**, *93*, 201.

(57) Fano, U. Effects of configuration interaction on intensities and phase shifts. *Phys. Rev.* **1961**, *124*, 1866.

(58) Feshbach, H. A unified theory of nuclear reactions. II. *Ann. Phys. (N.Y.)* **1962**, *19*, 287.

(59) Löwdin, P.-O. Studies in perturbation theory. IV. Solution of eigenvalue problem by projection operator formalism. *Journal Math. Phys.* **1962**, *3*, 969.

(60) Langhoff, P. W.; Corcoran, C. T. Stieltjes imaging of photoabsorption and dispersion profiles. *J. Chem. Phys.* **1974**, *61*, 146.

(61) Carravetta, V.; Ågren, H. Stieltjes imaging method for molecular Auger transition rates: Application to the Auger spectrum of water. *Phys. Rev. A* **1987**, *35*, 1022.

(62) Siegbahn, H.; Asplund, L.; Kelfve, P. The Auger electron spectrum of water vapour. *Chem. Phys. Lett.* **1975**, *35*, 330.

(63) Inhester, L.; Burmeister, C. F.; Groenhof, G.; Grubmüller, H. Auger spectrum of a water molecule after single and double core ionization. *J. Chem. Phys.* **2012**, *136*, 144304.

(64) Inhester, L.; Burmeister, C. F.; Groenhof, G.; Grubmüller, H. Erratum: "Auger spectrum of a water molecule after single and double core ionization" [J. Chem. Phys. 136, 144304 (2012)]. *J. Chem. Phys.* **2014**, *141*, 069904.

(65) Skomorowski, W.; Krylov, A. I. Feshbach–Fano approach for calculation of Auger decay rates using equation-of-motion coupled-cluster wave functions. I. Theory and implementation. *J. Chem. Phys.* **2021**, *154*, 084124.

(66) Skomorowski, W.; Krylov, A. I. Feshbach–Fano approach for calculation of Auger decay rates using equation-of-motion coupled-cluster wave functions. II. Numerical examples and benchmarks. *J. Chem. Phys.* **2021**, *154*, 084125.

(67) Fink, R. F.; Piancastelli, M. N.; Grum-Grzhimailo, A. N.; Ueda, K. Angular distribution of Auger electrons from fixed-in-space and rotating C1s$\rightarrow 2\pi$ photoexcited CO: Theory. *J. Chem. Phys.* **2009**, *130*, 014306.

(68) Averbukh, V.; Cederbaum, L. S. Ab initio calculation of interatomic decay rates by a combination of the Fano ansatz, Green's-function methods, and the Stieltjes imaging technique. *J. Chem. Phys.* **2005**, *123*, 204107.

(69) Kolorenč, P.; Averbukh, V. Fano-ADC(2,2) method for electronic decay rates. *J. Chem. Phys.* **2020**, *152*, 214107.

(70) McCurdy, C. W.; Rescigno, T. N. Extension of the method of complex basis functions to molecular resonances. *Phys. Rev. Lett.* **1978**, *41*, 1364.

(71) White, A. F.; Head-Gordon, M.; McCurdy, C. W. Complex basis functions revisited: Implementation with applications to carbon tetrafluoride and aromatic N-containing heterocycles within the static-exchange approximation. *J. Chem. Phys.* **2015**, *142*, 054103.

(72) White, A. F.; McCurdy, C. W.; Head-Gordon, M. Restricted and unrestricted non-Hermitian Hartree-Fock: Theory, practical considerations, and applications to metastable molecular anions. *J. Chem. Phys.* **2015**, *143*, 074103.

(73) White, A. F.; Epifanovsky, E.; McCurdy, C. W.; Head-Gordon, M. Second order Møller-Plesset and coupled cluster singles and doubles methods with complex basis functions for resonances in electron-molecule scattering. *J. Chem. Phys.* **2017**, *146*, 234107.

(74) Aguilar, J.; Combes, J.-M. A class of analytic perturbations for one-body Schrödinger Hamiltonians. *Commun. Math. Phys.* **1971**, *22*, 269.

(75) Balslev, E.; Combes, J.-M. Spectral properties of many-body Schrödinger operators with dilatation-analytic interactions. *Commun. Math. Phys.* **1971**, *22*, 280.

(76) Matz, F.; Jagau, T.-C. Molecular Auger decay rates from complex-variable coupled-cluster theory. *J. Chem. Phys.* **2022**, *156*, 114117.

(77) Matz, F.; Jagau, T.-C. Channel-specific core-valence projectors for determining partial Auger decay widths. *Mol. Phys.* **2022**, *120*, e2105270.

(78) Karippara Jayadev, N.; Ferino-Pérez, A.; Matz, F.; Krylov, A. I.; Jagau, T.-C. The Auger spectrum of benzene. *J. Chem. Phys.* **2023**, *158*, 064109.

(79) Emrich, K. An extension of the coupled cluster formalism to excited states (I). *Nucl. Phys. A* **1981**, *351*, 379.

(80) Sekino, H.; Bartlett, R. J. A linear response, coupled-cluster theory for excitation energy. *Int. J. Quant. Chem.* **1984**, *26*, 255.

(81) Stanton, J. F.; Bartlett, R. J. The equation of motion coupled-cluster method. A systematic biorthogonal approach to molecular excitation energies, transition probabilities, and excited state properties. *J. Chem. Phys.* **1993**, *98*, 7029.

(82) Krylov, A. I. Equation-of-motion coupled-cluster methods for open-shell and electronically excited species: The hitchhiker's guide to Fock space. *Annu. Rev. Phys. Chem.* **2008**, *59*, 433.

(83) Shavitt, I.; Bartlett, R. J. *Many-body methods in chemistry and physics: MBPT and coupled-cluster theory*; Cambridge University Press, 2009.

(84) Stanton, J. F.; Gauss, J. Analytic energy derivatives for ionized states described by the equation-of-motion coupled cluster method. *J. Chem. Phys.* **1994**, *101*, 8938.

(85) Nooijen, M.; Bartlett, R. J. Similarity transformed equation-of-motion coupled-cluster theory: Details, examples, and comparisons. *J. Chem. Phys.* **1997**, *107*, 6812.

(86) Sattelmeyer, K. W.; Schaefer, H. F.; Stanton, J. F. Use of 2h and 3h-p-like coupled-cluster Tamm–Dancoff approaches for the equilibrium properties of ozone. *Chem. Phys. Lett.* **2003**, *378*, 42.

(87) Cederbaum, L. S.; Zobeley, J.; Tarantelli, F. Giant intermolecular decay and fragmentation of clusters. *Phys. Rev. Lett.* **1997**, *79*, 4778.

(88) Jahnke, T.; Hergenhahn, U.; Winter, B.; Dörner, R.; Frühling, U.; Demekhin, P. V.; Gokhberg, K.; Cederbaum, L. S.; Ehresmann, A.; Knie, A. et al. Interatomic and intermolecular Coulombic decay. *Chem. Rev.* **2020**, *120*, 11295.

(89) Zuev, D.; Jagau, T.-C.; Bravaya, K. B.; Epifanovsky, E.; Shao, Y.; Sundstrom, E.; Head-Gordon, M.; Krylov, A. I. Complex absorbing potentials within EOM-CC family of methods: Theory, implementation, and benchmarks. *J. Chem. Phys.* **2014**, *141*, 024102.

(90) Bravaya, K. B.; Zuev, D.; Epifanovsky, E.; Krylov, A. I. Complex-scaled equation-of-motion coupled-cluster method with single and double substitutions for autoionizing excited states: Theory, implementation, and examples. *J. Chem. Phys.* **2013**, *138*, 124106.

(91) Epifanovsky, E.; Gilbert, A. T. B.; Feng, X.; Lee, J.; Mao, Y.; Mardirossian, N.; Pokhilko, P.; White, A. F.; Coons, M. P.; Dempwolff, A. L. et al. Software for the frontiers of quantum chemistry: An overview of developments in the Q-Chem 5 package. *J. Chem. Phys.* **2021**, *155*, 084801.

(92) Moiseyev, N.; Certain, P. R.; Weinhold, F. Resonance properties of complex-rotated hamiltonians. *Mol. Phys.* **1978**, *36*, 1613.

(93) Tarantelli, F.; Sgamellotti, A.; Cederbaum, L. S.; Schirmer, J. Theoretical investigation of many dicationic states and the Auger spectrum of benzene. *J. Chem. Phys.* **1987**, *86*, 2201.

(94) McGuire, E. J. K-Shell Auger transition rates and fluorescence yields for elements Be-Ar. *Phys. Rev.* **1969**, *185*, 1.

(95) Hasoğlu, M. F.; Nikolić, D.; Gorczyca, T. W.; Manson, S. T.; Chen, M. H.; Badnell, N. R. Nonmonotonic behavior as a function of nuclear charge of the K-shell Auger and radiative rates and fluorescence yields along the $1s2s^22p^3$ isoelectronic sequence. *Phys. Rev. A* **2008**, *78*, 032509.

(96) Ågren, H. On the interpretation of molecular valence Auger spectra. *J. Chem. Phys.* **1981**, *75*, 1267.

(97) Thissen, R.; Delwiche, J.; Robbe, J. M.; Duflot, D.; Flament, J. P.; Eland, J. H. D. Dissociations of the ethyne dication $C_2H_2^{2+}$. *J. Chem. Phys.* **1993**, *99*, 6590.

(98) Agren, H.; Vahtras, O. Spin-orbit coupling in molecular Auger spectra: propensity rules tested for water. *J. Phys. B–At. Mol. Opt.* **1993**, *26*, 913.

(99) Cederbaum, L. S.; Tarantelli, F. Nuclear dynamics of several decaying overlapping electronic states: A time-dependent formulation. *J. Chem. Phys.* **1993**, *99*, 5871.

(100) Holzmeier, F.; Wolf, T. J. A.; Gienger, C.; Wagner, I.; Bozek, J.; Nandi, S.; Nicolas, C.; Fischer, I.; Gühr, M.; Fink, R. F. Normal and resonant Auger spectroscopy of isocyanic acid, HNCO. *The Journal of Chemical Physics* **2018**, *149*.

TOC Graphic